JOURNAL OF GEOPHYSICAL RESEARCH, VOL. 103, NO. D24, PAGES 31,637–31,645, DECEMBER 27, 1998

Radiative forcing by mineral dust aerosols: sensitivity to key variables

H. Liao and J.H. Seinfeld

Division of Engineering and Applied Science, California Institute of Technology, Pasadena

Abstract. We examine diurnally averaged radiative forcing by mineral dust aerosols in shortwave and longwave spectral regions using a one-dimensional column radiation model. At the top of the atmosphere (TOA), net (shortwave plus longwave) dust radiative forcing can be positive (heating) or negative (cooling) depending on values of key variables. We derive an analytical expression for the critical single-scattering albedo at which forcing changes sign for an atmosphere containing both cloud and aerosol layers. At the surface, net dust forcing can be positive or negative under clear-sky conditions, whereas it is always cooling in the presence of a low-level stratus cloud. Longwave radiative forcing is essentially zero when clouds are present. We also study the sensitivity of dust diurnally averaged forcing to the imaginary part of refractive index (k), height of the dust layer, dust particle size, and dust optical depth. These variables play different roles as follows: (1) under both clear- and cloudy sky conditions, net TOA forcing is more sensitive to k than net surface forcing; (2) clear-sky longwave forcing and cloudy-sky TOA shortwave forcing are very sensitive to the altitude of the dust layer; although clear-sky shortwave forcing is not sensitive to it; (3) clear-sky shortwave forcing is much more sensitive to particle size than cloudy-sky shortwave forcing; longwave forcing is not sensitive to particle size; and (4) all forcings are sensitive to optical depth except cloudy-sky longwave forcing.

1. Introduction

Among the aerosol constituents of the Earth's atmosphere, those with the most poorly characterized and most variable optical properties are the mineral dusts from deserts and arid regions. The magnitude of global mean radiative forcing by mineral dust has been estimated to be comparable to that of anthropogenic aerosols [*Sokolik and Toon*, 1996]. Early studies of dust radiative effects were performed in the 1980s [*Carlson and Benjamin*, 1980] and in the context of nuclear winter scenarios [*Ramaswamy and Kiehl*, 1985; *Cess*, 1985]. *Tegen and Lacis* [1996] showed that the sign of total (shortwave plus longwave) radiative forcing at the tropopause can be either positive (warming) or negative (cooling) depending on the particle size and vertical distribution of the dust layer. Furthermore, using a general circulation model (GCM), *Tegen et al.* [1996] calculated the top of atmosphere (TOA) radiative forcing of mineral dust aerosol and found that forcing at solar wavelengths can be either positive or negative, depending on clear versus cloudy sky conditions and on the local surface albedo. *Sokolik et al.* [1998] have studied the importance of mineral dust radiative forcing at infrared wavelengths.

Because of its importance in global radiative forcing by aerosols and because of the considerable uncertainty attending the magnitude of that forcing, we systematically examine here, using a one-dimensional radiative transfer model, the sensitivity of dust radiative forcing to its physical and optical properties, the vertical distribution of dust in the atmosphere, surface albedo, and to the presence or absence of clouds. Our goal is both to define regions of forcing behavior (positive or negative forcing) and to establish the quantitative sensitivity of forcing to uncertainties in essential variables.

Paper number 1998JD200036.
0148-0227/98/1998JD200036$09.00

2. Radiative Transfer Model

The radiative transfer model of *Fu and Liou* [1993] calculates shortwave fluxes over six solar bands (0.2-0.7, 0.7-1.3, 1.3-1.9, 1.9-2.5, 2.5-3.5, and 3.5-4.0 μm) and longwave fluxes over 12 infrared spectral intervals (2200-1900, 1900-1700, 1700-1400, 1400-1250, 1250-1100, 1100-980, 980-800, 800-670, 670-540, 540-400, 400-280, and 280-0 cm^{-1}). The model includes molecular Rayleigh scattering, gaseous absorption, and cloud effects; we have extended the model to include aerosol absorption and scattering. The atmosphere is divided into 98 layers, with a vertical resolution of 100 m near the cloud layer and of 1 km at other altitudes. Vertical profiles of pressure, temperature, ozone, and H_2O vapor mixing ratios are from U.S. Standard Atmosphere (1976). The solar constant is 1376 W m^{-2}.

Mie theory is used to calculate the optical properties of dust aerosols. For each solar band i of the radiative code, single-scattering albedo is calculated by integrating over the band as $\omega_i = \int W(\lambda)\omega d\lambda / \int W(\lambda) d\lambda$, where $W(\lambda)$ is the incident solar flux at the top of the atmosphere; for each longwave band, $\omega_i = \int \omega d\lambda / \int d\lambda$. The extinction cross section and asymmetry factor are also calculated in the same manner.

Both diurnally averaged TOA and surface radiative forcing are examined in this work. Letting $\Delta F(\mu_0)$ denote the radiative forcing, where μ_0 is the cosine of the solar zenith angle, the diurnally averaged forcing $\Delta\overline{F}$ is calculated by [*Cess*, 1985]

$$\Delta\overline{F} = \frac{1}{2}\int_0^1 \Delta F(\mu_0)\, d\mu_0 \qquad (1)$$

For surface forcing, ΔF is defined as $\left(F_S^d - F_S^0\right)$ for clear-sky conditions and $\left(F_S^{c+d} - F_S^c\right)$ for cloudy-sky conditions,

where F_S^0 and F_S^d are the net fluxes (downward is positive) at the surface for dust-free and dust-laden cases, respectively; F_S^c and F_S^{c+d} are net fluxes at the surface for cloudy sky without dust and cloudy sky with dust, respectively. For TOA forcing, ΔF is defined as $-(F_{\mathrm{TOA}}^d \uparrow - F_{\mathrm{TOA}}^0 \uparrow)$ for clear-sky conditions and $-(F_{\mathrm{TOA}}^{c+d} \uparrow - F_{\mathrm{TOA}}^c \uparrow)$ for cloudy sky conditions, where $F_{\mathrm{TOA}}^0 \uparrow$ and $F_{\mathrm{TOA}}^d \uparrow$ are the upward fluxes at TOA for dust-free and dust-laden cases, respectively; $F_{\mathrm{TOA}}^c \uparrow$ and $F_{\mathrm{TOA}}^{c+d} \uparrow$ are upward fluxes at TOA for cloudy sky without dust and cloudy sky with dust, respectively. The negative sign implies that if $F_{\mathrm{TOA}}^d \uparrow > F_{\mathrm{TOA}}^0 \uparrow$, aerosols produce a cooling effect at TOA and vice versa.

3. Basis of the Analysis

We apply the one-dimensional radiative transfer model to examine the sensitivity of mineral dust radiative forcing to variation in key parameters. A uniform dust layer with column burden of 100 mg m^{-2} is assumed. On the basis of the analysis of *Dentener et al.* [1996], 100 mg m^{-2} is roughly the annual average column dust burden over North Africa and Asia. The optical depth of the dust layer depends on particle size; for a column burden of 100 mg m^{-2}, the optical depth is 0.02 (in the wavelength band 0.2 to 0.7 μm) for a dust mass median diameter of 8 μm and 0.21 (in the same wavelength band) for a mass median diameter of 1 μm. Three different altitudes for the dust layer will be considered: 0-3 km, 0-1 km, and 3-6 km. The cloud layer, when present, is highly simplified; we assume the layer is vertically uniform and is located between 1 and 1.5 km, with a liquid water content of 0.2 g m^{-3} and an effective cloud drop radius of 10 μm. The optical depth of the cloud layer is 15.5 in the wavelength band of 0.2 to 0.7 μm. Since we are concerned here principally with the radiative interaction between cloud and dust layers, it is sufficient to consider such a simplified cloud layer. Dust particles are assumed to be spherical, having a mass distribution that is lognormal with geometric standard deviation of 2.0. The dust mass median diameter will be varied over the range of 1.0 to 8.0 μm. Dust density is taken to be 2.5 g cm^{-3}. (*Tegen and Fung* [1994] assumed 2.5-2.65 g cm^{-3} for different dust particle size classes.) It should be noted that the assumption of particle sphericity may not lead to significant errors for a climate forcing calculation since integration over the entire hemisphere is performed [*Mishchenko*, 1993; *Mishchenko and Travis*, 1994; *Lacis and Mishchenko*, 1995]. For satellite data retrieval, on the other hand, properly accounting for the nonspherical nature of particles is necessary.

There is significant variation in the refractive index of dust aerosol from the world's desert regions, especially the imaginary component k [*Patterson et al.*, 1977; *Sokolik et al.*, 1993, 1998]. We select for the base case refractive indices that lie at about the average values of a variety of measurements; we use curve 8 in Figure 1 of *Sokolik et al.* [1993] for k in the shortwave wavelength region and curve 5 in Figure 1a of *Sokolik et al.* [1998] for k in the longwave region. Thus k is 0.006 and 0.25 at the wavelengths of 0.5 μm and 10 μm, respectively. Although values of the real part of the refractive index also vary, the value of 1.5 chosen here is relatively representative of many dusts and is not varied in our study.

The sensitivity of diurnally averaged forcing to key variables is studied in two ways. First, overall sensitivity is evaluated by examining the dependence of diurnally averaged forcing on key variables. Second, the local sensitivity, the derivative of forcing with respect to parameters that may vary, is calculated as follows. The local sensitivity of diurnally averaged radiative forcing (at TOA or surface) to a parameter x is $x\frac{\partial \Delta \bar{F}}{\partial x}$ (approximated by $x\frac{\Delta \bar{F} \mid \Delta x + \Delta x - \Delta \bar{F} \mid x - \Delta x}{2\Delta x}$) [*Chylek and Kiehl*, 1981], where x represents, in the current case, variables such as refractive index, mass median diameter, and dust optical depth; the overall quantity is the change in radiative forcing (in W m^{-2}) per fractional change in x.

4. Dependence of Diurnally Averaged Radiative Forcing on Key Variables

4.1. Dependence of Radiative Forcing on Surface Albedo

Figure 1 shows diurnally averaged TOA and surface shortwave forcing in the absence and presence of a cloud layer as a function of surface albedo r_S. The dust layer is located at 0-3 km and dust mass median diameter is 3.5 μm. Clear-sky TOA shortwave forcing increases from negative (cooling) to positive (heating) as surface albedo increases, whereas TOA forcing in the presence of the cloud layer is positive for all surface reflectances. High-albedo surfaces and/or the presence of a cloud layer lead to enhanced absorption of reflected radiation thus producing heating at TOA. Surface shortwave forcing of mineral dust aerosol is negative under both clear and cloudy sky conditions. The magnitude of cooling under clear-sky conditions decreases as surface albedo increases. This behavior can be understood by examining the definition for surface shortwave forcing, $\left(F_S^d - F_S^0\right)$, which can be expressed as $\left(1 - r_S\right)\left(F_S^d \downarrow - F_S^0 \downarrow\right)$, where $F_S^0 \downarrow$ and $F_S^d \downarrow$ are the downward shortwave fluxes at the surface for dust-free and dust-laden cases, respectively. When surface albedo increases, the magnitude of $\left(F_S^d \downarrow - F_S^0 \downarrow\right)$ decreases (smaller negative value) as a result of

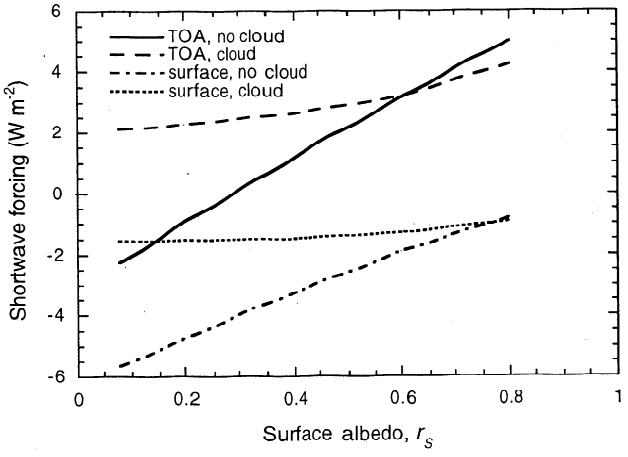

Figure 1. TOA and surface diurnally averaged shortwave dust forcing as a function of surface albedo r_S under cloud-free and cloud conditions. Dust layer of total column burden 100 mg m^{-2} located over 0-3 km altitude. Mass distribution of dust log-normally distributed with mass median diameter of 3.5 μm and geometric standard deviation of 2.0.

multiple scattering between aerosol and surface, and the factor $(1-r_s)$ also decreases; thus under clear-sky conditions, the surface experiences less cooling at higher surface albedo. Cloudy sky surface shortwave forcing is defined as $(F_s^{c+d} - F_s^c)$, which can be written as $(1-r_s)(F_s^{c+d}\downarrow - F_s^c\downarrow)$, where $F_s^c\downarrow$ and $F_s^{c+d}\downarrow$ are downward solar fluxes at the surface for cloudy sky without dust and cloudy sky with dust, respectively. As surface albedo increases, even though $(1-r_s)$ decreases rapidly, $(F_s^{c+d}\downarrow - F_s^c\downarrow)$ increases in magnitude at about the same rate (greater negative value), leading to the net effect that surface shortwave cooling under cloudy sky conditions is relatively independent of surface albedo for $0.08 < r_s < 0.8$. It is important to note that over ocean and normal land surfaces ($r_s < 0.4$), the magnitude of surface forcing under cloudy sky conditions is considerably smaller than that under clear sky conditions; at a surface albedo of 0.20, for example, surface forcing of dust is about -4.7 W m^{-2} in the absence of the cloud layer and -1.5 W m^{-2} in its presence.

Longwave radiative forcing is independent of surface albedo and is positive (heating) at both TOA and surface. For the conditions assumed here, TOA longwave forcing is 0.40 W m^{-2}, and surface longwave is 1.30 W m^{-2} for clear-sky conditions, and both TOA and surface longwave forcing are 0.10 W m^{-2} when the cloud layer is present. The fact that the cloud layer greatly reduces both TOA and surface longwave forcing will be addressed subsequently.

4.2. Dependence of Radiative Forcing on Altitude of the Dust Layer

Although mineral dust generally resides in the lowest several kilometers of the atmosphere, dust particles can be transported to high altitudes. To examine the effect of dust layer altitude on radiative forcing, we consider the vertically uniform dust layer of fixed column burden 100 mg m^{-2} occupying each of three altitude ranges: 0-3 km, 0-1 km, and 3-6 km. Dust mass median diameter is assumed to be 3.5 μm.

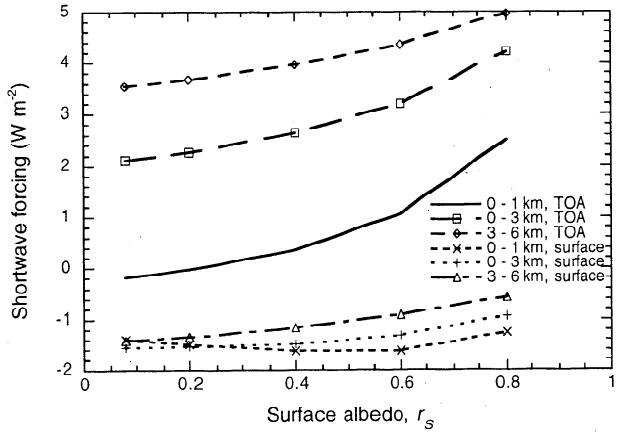

Figure 2. Cloudy-sky TOA and surface diurnally averaged shortwave dust forcing as a function of surface albedo r_s for different assumed dust layer altitudes. Cloud layer of liquid water content 0.2 g m^{-3} and effective droplet radius 10 μm located between 1 and 1.5 km altitude. Dust layer of total column burden 100 mg m^{-2}. Mass distribution of dust lognormally distributed with mass median diameter of 3.5 μm and geometric standard deviation of 2.0.

Table 1. Diurnal-Average Longwave Radiative Forcing Under Cloud-Free and Cloud Conditions

Dust Layer Altitude, km	Without Cloud, W m^{-2}		With Cloud, W m^{-2}	
	TOA	Surface	TOA	Surface
0-1	0.2	1.4	0.0	0.1
0-3	0.4	1.3	0.1	0.1
3-6	1.0	0.9	0.6	0.0

In the absence of clouds, shortwave forcing is not sensitive to the altitude of the dust layer; both TOA and surface shortwave forcing are about the same as those with the dust layer at 0-3 km (see Figure 1). In the presence of a cloud layer, TOA warming is strongest when the dust layer lies above the cloud layer (Figure 2), since the dust absorbs both incoming solar radiation and that reflected by the cloud layer [*Crisp*, 1997; *Haywood and Shine*, 1997; *Hansen et al.*, 1997].

With 50% of total column burden located above cloud, TOA forcing of a dust layer at 0-3 km is about 2 W m^{-2} larger than that of a dust layer at 0-1 km and about 1.5 W m^{-2} lower than that of a dust layer at 3-6 km. The three lines for TOA forcing tend to converge when surface albedo is high ($r_s > 0.6$) because the high-albedo surface leads to more absorption of radiation by aerosols below the cloud layer. When the dust layer lies completely beneath cloud, TOA shortwave forcing changes sign as r_s increases, being negative over low-albedo surfaces and positive over high-albedo surfaces.

Surface shortwave forcing under cloudy sky conditions is not so sensitive to the altitude of the dust layer as TOA shortwave forcing, especially over low-albedo surfaces ($r_s < 0.3$). Surfaces with higher albedo ($r_s > 0.3$) lead to stronger multiple scattering among surface, cloud and dust aerosol, as well as more absorption along the optical path. When the dust layer is located below the cloud layer (0-1 km), multiple scattering produces the strongest cooling for high-albedo surfaces.

Longwave radiative forcing for the three dust layer altitudes is given in Table 1. Under clear sky conditions, the higher the dust layer, the larger the TOA forcing but the smaller the surface forcing. The temperature of the dust layer is lower the higher its altitude; thus emission of longwave radiation is smaller, so less longwave radiation both escapes to space and arrives at the surface. In the presence of a cloud layer, both TOA and surface longwave forcing are practically negligible in all cases, except for the case when the dust layer is completely above cloud (at 3-6 km altitude). When cloud overlays the dust layer, it absorbs the IR radiation emitted by the dust layer and emits longwave radiation at its top. Since the temperature at the top of the cloud layer is assumed to be the same both with and without dust, TOA IR forcing is zero on the basis of our definition of forcing. When the dust layer is above cloud at 3-6 km, IR forcing still exists, but the magnitude is smaller compared with that under clear-sky conditions, because the temperature at the top of the cloud is lower than that at the surface. Surface longwave forcing in the presence of the cloud layer is essentially zero because the effect

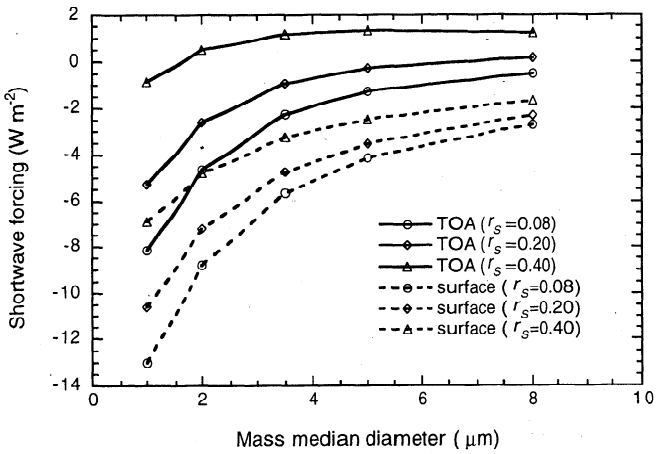

Figure 3. TOA and surface diurnally averaged shortwave dust forcing as a function of dust mass median diameter and surface albedo r_S under cloud-free conditions. Dust layer of total column burden 100 mg m^{-2} located over 0-3 km altitude. Mass distribution of dust lognormally distributed with geometric standard deviation of 2.0.

of dust aerosol above the cloud is blocked by the cloud, while the aerosols below cloud cannot exert forcing on the surface as the particles have about the same temperature as the cloud bottom.

4.3. Dependence of Radiative Forcing on Dust Mass Median Diameter

To examine the effect of aerosol size on dust radiative forcing, we vary the mass median diameter of the dust layer from 1.0 μm to 8.0 μm to span the range from long-lived, transported dust to that at source regions. The column burden and altitude of the dust layer are fixed at 100 mg m^{-2} and 0-3 km, respectively.

Diurnally averaged shortwave forcing as a function of dust mass median diameter and surface albedo is shown for clear and cloudy conditions in Figures 3 and 4, respectively. Under clear-sky conditions, as mass median diameter increases, shortwave forcing tends toward warming, which is in agreement with the results obtained by *Tegen and Lacis* [1996]. Negative forcing decreases in magnitude or positive forcing increases in magnitude as mass median diameter increases from 1 μm to 5 μm, whereas both TOA and surface forcing change more slowly when mass median diameter exceeds 5 μm. The fact that shortwave forcing is very sensitive to mass median diameter in the 1.0 to 5.0 μm region indicates that this will be a key variable in global mineral dust forcing simulations, since about 90% of global dust mass loading is assumed to lie in this size region [*Tegen and Lacis*, 1996].

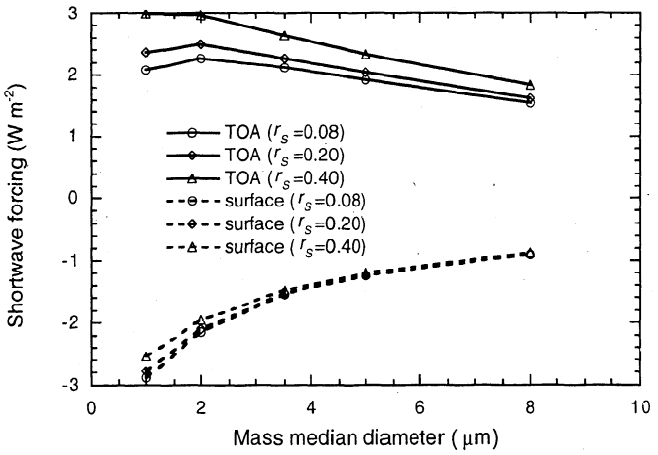

Figure 4. TOA and surface diurnally averaged shortwave dust forcing at as a function of dust mass median diameter and surface albedo r_S in the presence of a cloud layer. Cloud layer of liquid water content 0.2 g m^{-3} and effective droplet radius 10 μm located between 1 and 1.5 km altitude. Dust layer of total column burden 100 mg m^{-2} located over 0-3 km altitude. Mass distribution of dust lognormally distributed with geometric standard deviation of 2.0.

Table 2. Diurnal-Average Longwave Radiative Forcing Under Cloud-Free and Cloud Conditions.

Mass Median Diameter μm	Without Cloud, W m^{-2}		With Cloud, W m^{-2}	
	TOA	Surface	TOA	Surface
1.0	0.2	1.0	0.0	0.1
2.0	0.4	1.2	0.0	0.1
3.5	0.4	1.3	0.1	0.1
5.0	0.5	1.3	0.1	0.1
8.0	0.4	1.1	0.1	0.1

In contrast to the clear-sky case, in the presence of a cloud layer, TOA forcing is always positive (heating), with the maximum forcing occurring at a dust mass median diameter of about 2.0 μm for $r_S \leq 0.4$. The reason that the maximum positive TOA forcing occurs at a mass median diameter of about 2.0 μm can be explained as follows. At solar wavelengths, the single-scattering albedo ω decreases with increasing particle size [*Tegen and Lacis*, 1996]. When the dust mass median diameter exceeds about 2 μm at a fixed mass loading, however, the effect of absorption begins to decrease strongly because the total particle number concentration falls off rapidly. For the conditions assumed here, for example, dust number concentration is 28 cm^{-3} at a mass median diameter of 2 μm, whereas it is 5 cm^{-3} at a mass median diameter of 3.5 μm.

Longwave forcing for different mass median diameters is given in Table 2. For clear-sky conditions, both TOA and surface longwave forcing increases with increasing mass median diameter, reaching a maximum at 5 μm and then decreasing with further increase in mass median diameter. This behavior is a result of a similar variation in extinction coefficient (thus optical depth) in the wavelength region of 4-12 μm. When clouds are present, the dust layer exerts nearly zero forcing at both TOA and surface, regardless of particle size distribution.

4.4. Dependence of Radiative Forcing on Dust Optical Depth

Radiative forcing as a function of dust optical depth is shown under clear and cloudy conditions in Figures 5 and 6, respectively. A mass median diameter of 3.5 μm is assumed, and the altitude of the dust layer is fixed at 0-3 km. Under both clear and cloudy conditions, radiative forcing (longwave and shortwave) varies more or less linearly with optical depth at surface albedos characteristic of both ocean (r_S = 0.08) and land (r_S = 0.2) surfaces.

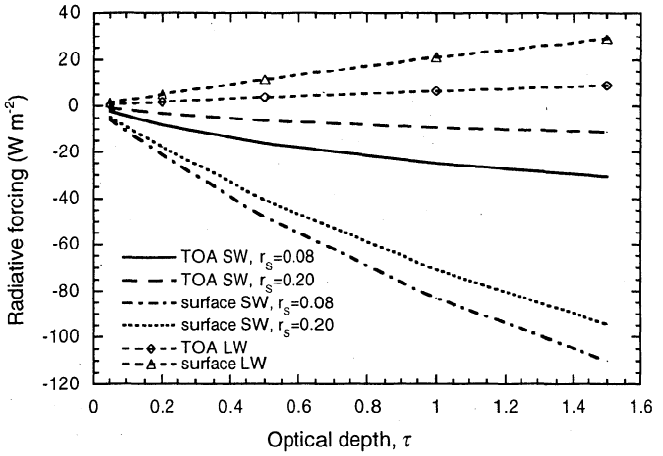

Figure 5. TOA and surface diurnally averaged dust radiative forcing (shortwave (SW) and longwave (SW)) as a function of dust optical depth under cloud-free conditions. Dust layer of total column burden 100 mg m^{-2} located over 0-3 km altitude. Mass distribution of dust lognormally distributed with mass median diameter of 3.5 μm and geometric standard deviation of 2.0.

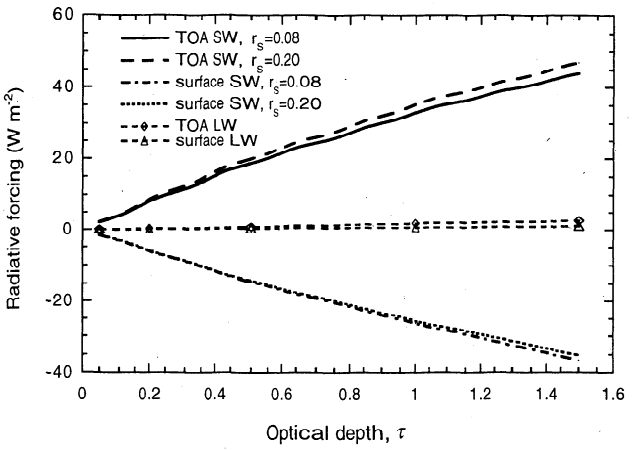

Figure 6. TOA and surface diurnally averaged dust radiative forcing (shortwave (SW) and longwave (SW)) as a function of dust optical depth in the presence of a cloud layer. Cloud layer of liquid water content 0.2 g m^{-3} and effective droplet radius 10 μm located between 1 and 1.5 km altitude. Dust layer of total column burden 100 mg m^{-2} located over 0-3 km altitude. Mass distribution of dust lognormally distributed with mass median diameter of 3.5 μm and geometric standard deviation of 2.0.

4.5. Dependence of Longwave Forcing on Atmospheric Conditions

We have seen that clear-sky longwave forcing depends on dust layer altitude, dust mass median diameter, and dust optical depth. Longwave radiative forcing also depends on atmospheric conditions, such as temperature profile and water vapor content (Table 3). Clear-sky longwave forcing is sensitive to changes in the atmospheric temperature profile. In cases in which we vary atmospheric temperature profile, the surface temperature is changed accordingly, thus the relative temperatures of dust layer, surface, and cloud remain the same. If the change in temperature is not uniform throughout the atmosphere, one can expect a larger or smaller sensitivity of longwave forcing to the actual temperature profile [*Ramanathan*, 1977]. Water vapor content is also a key parameter that affects longwave forcing. By setting the water vapor mixing ratio in the lowest 2.5 km of the U. S. Standard Atmosphere to be 2.4 g kg^{-1} ("dry case") and 8.0 g kg^{-1} ("wet case"), under clear sky conditions, TOA longwave forcing

Table 3. Longwave Forcing (W m^{-2}) for Different Assumptions Concerning Atmospheric Conditions

Surface Temperature	Temperature Profile	Water Vapor Profile	Longwave Forcing (W m^{-2})			
			No Cloud		Cloud	
K			TOA	Surface	TOA	Surface
		Sensitivity to the Atmospheric Temperature Profile				
298	increase 10 K throughout U. S. Standard profile	U. S. Standard Atmosphere	0.5	1.6	0.1	0.1
278	decrease 10 K throughout U. S. Standard profile	U. S. Standard Atmosphere	0.3	1.0	0.0	0.0
		Sensitivity to the Atmospheric Water Vapor Profile				
288	U. S. Standard Atmosphere	dry case[a]	0.5	1.5	0.1	0.1
288	U. S. Standard Atmosphere	wet case[b]	0.2	0.8	0.1	0.0

[a] Dry case has the same vertical characteristics as the U. S. Standard atmosphere except the water vapor mixing ratio is lower (assumed to be 2.4 g/kg) in the lowest 2.5 km.

[b] Wet case has the same vertical characteristics as the U. S. Standard Atmosphere except the water vapor mixing ratio is higher (assumed to be 8.0 g/kg) in the lowest 2.5 km.

is 0.5 and 0.2 W m^{-2} (25% and -50% change with respect to the base case), and surface forcing is 1.5 and 0.8 W m^{-2} (15% and -38% change with respect to base case) for dry and wet cases, respectively. Thus the drier the atmosphere, the stronger the longwave radiative forcing of dust, a conclusion that is consistent with results presented by *Sokolik et al.* [1998].

5. Local Sensitivity of Mineral Dust Radiative Forcing to Refractive Index, Mass Median Diameter and Optical Depth

Of the variables considered in this study, the most uncertain are imaginary part of the mineral dust refractive index (k), dust mass median diameter (D_{pm}), and dust optical depth (τ). To evaluate the relative sensitivity of the diurnally averaged radiative forcing to these variables, local sensitivity coefficients, as described in section 3, are computed at the base case conditions.

The base case for the sensitivity study assumes that a dust layer of total column burden of 100 mg m^{-2} is located over 0-3 km altitude, with mass median diameter of 3.5 μm. By varying x (x represents k, D_{pm}, and τ) of the base case by 20% (-10% to +10%), we obtain the local sensitivity $x\frac{\partial \Delta \overline{F}}{\partial x}$ over ocean (r_s = 0.08) and land surfaces (r_s = 0.20).

Table 4 shows the local sensitivity of diurnally averaged radiative forcing to k. We note that TOA shortwave forcing under cloudy sky conditions is more sensitive to k than that under clear-sky conditions, as the cloud layer enhances aerosol absorption above the cloud, thus accentuating the effect of k. On the contrary, surface shortwave forcing is more sensitive to k in the absence of the cloud layer than in its presence. For the conditions assumed here, the effect of k on TOA and surface longwave forcing is nonzero only for clear-sky conditions. For net (shortwave plus longwave) forcing, no matter whether clouds are present or not, TOA forcing is more sensitive to variations in k than surface forcing.

The local sensitivity of diurnally averaged radiative forcing to D_{pm} is summarized in Table 5. Shortwave forcing at both TOA and surface in the absence of the cloud layer is much more sensitive to size than when clouds are present, and longwave forcing is not sensitive to particle size at fixed dust column burden.

Sensitivity of radiative forcing to dust optical depth is summarized in Table 6. All forcings, except longwave forcing in the presence of clouds, are sensitive to optical depth.

Table 4. Radiative Forcing Sensitivity $k(\partial \Delta \overline{F}/\partial k)$ With Respect to the Imaginary Part of the Refractive Index k

Surface Albedo	*TOA Sensitivities*		*Surface Sensitivities*	
	No cloud	Cloud	No cloud	Cloud
	Shortwave			
0.08	0.83	1.81	-1.54	-0.83
0.20	1.18	1.97	-1.40	-0.86
	Longwave			
	0.5	0	1.0	0
	Net (Shortwave + Longwave)			
0.08	1.23	1.81	-0.54	-0.83
0.20	1.68	1.97	-0.40	-0.86

$\Delta \overline{F}$ is given in W m^{-2}. (Positive values imply that the increase in k produces larger heating or less cooling, while negative values mean less heating or larger cooling.) Base value of k is 0.006 and 0.25 at the wavelengths of 0.5 μm and 10 μm, respectively.

Table 5. Radiative Forcing Sensitivity $D_{pm}(\partial \Delta \overline{F}/\partial D_{pm})$ With Respect to the Mass Median Diameter D_{pm}

Surface Albedo	*No Cloud*		*Cloud*	
	TOA	Surface	TOA	Surface
	Shortwave			
0.08	3.45	4.95	-0.50	0.95
0.20	2.35	3.90	-0.55	0.90
	Longwave			
	0.5	0	0	0

$\Delta \overline{F}$ is given in W m^{-2}. (Positive values imply that the increase in D_{pm} produces larger heating or less cooling, while negative values mean less heating or larger cooling.) Base value of D_{pm} is 3.5 μm.

6. Critical Single-Scattering Albedo

A first-order estimate of TOA shortwave radiative forcing can be made by calculating the change in planetary albedo resulting from addition of an optically thin aerosol layer. The critical single-scattering albedo ω_{crit}, of an optically thin aerosol layer at which the perturbation in planetary albedo changes from one of cooling to one of heating, is given by [*Chylek and Coakley,* 1974; *Seinfeld and Pandis,* 1998]

$$\omega_{crit} = \frac{2r_s}{2r_s + \beta(1 - r_s)^2} \qquad (2)$$

where β is the upscatter fraction of the particles. Values of $\omega > \omega_{crit}$ lead to cooling; values of $\omega < \omega_{crit}$ to heating.

Table 6. Radiative Forcing Sensitivity $\tau(\partial \Delta \overline{F}/\partial \tau)$ With Respect to Optical Depth τ

Surface Albedo	*No Cloud*		*Cloud*	
	TOA	Surface	TOA	Surface
	Shortwave			
0.08	-1.90	-5.22	2.01	-1.50
0.20	-0.75	-4.37	2.15	-1.48
	Longwave			
	0.40	1.23	0.10	0.03

$\Delta \overline{F}$ is given in W m^{-2}. (Positive values imply that the increase in τ produces larger heating or less cooling, while negative values mean less heating or larger cooling.) Base value of τ is 0.05.

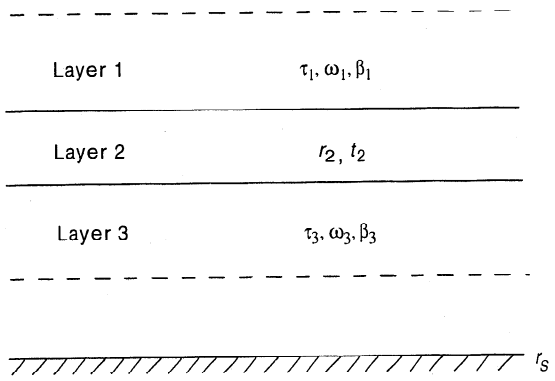

Figure 7. Three-layer radiative model of atmosphere. Layers 1 and 3 are aerosol layers, with optical depths, single scattering albedos, and upscatter fractions indicated. Layer 2 is the cloud layer, with albedo r_2 and transmittance t_2.

The analysis that leads to equation (2) can be extended to the case of interspersed aerosol and cloud layers (Figure 7). Layers 1 and 3 are aerosol layers, the optical properties of which are characterized by optical depths τ_1 and τ_3, single-scattering albedo ω, and upscatter fraction β. Layer 2 is a cloud layer with albedo r_2 and transmittance t_2. The Earth's surface is considered as a Lambertian reflector with albedo r_S. If aerosol exists entirely above cloud, then $\tau_3 = 0$; conversely, for an aerosol layer wholly below cloud, $\tau_1 = 0$. We show in the Appendix that the critical single-scattering albedo of the aerosol in this general case is

$$\omega_{crit} = \frac{\left(r_2 + \frac{r_S t_2^2}{1 - r_2 r_S}\right) + r_S^2 r_2 t_2^2 - r_2(1 + r_S^2 t_2^2)(1 - 4\tau_1) - r_S t_2^2 (1 + r_S r_2)(1 - 4\tau)}{2(1 + r_S^2 t_2^2)[\tau_1\beta + 2r_2(1-\beta)\tau_1 + r_2^2\tau_1\beta + \tau_3\beta_3^2] + r_S t_2^2 (1 + r_S r_2)[4(1-\beta)\tau + 4\beta\tau_2]} \quad (3)$$

Generally β_1 and β_3 should be different because the incident irradiance on the top of layer 1 is direct while that on the top of layer 3 is mainly diffuse. The analysis in the Appendix considers $\beta_1 \neq \beta_3$; for simplicity we assume $\beta_1 = \beta_3 = \beta$ in equation (3).

The critical single-scattering albedo obtained by equation (3) is shown in Figure 8 as a function of surface albedo r_S. As in previous sections, the cloud layer with liquid water content of 0.2 g m^{-3} and effective droplet radius 10 μm is located between 1 and 1.5 km altitude. Based on our calculations, the albedo r_2 and transmission t_2 of the cloud, which are computed by assuming the surface albedo $r_S = 0$ and integrated over all angles of incoming radiation, are 0.61 and 0.32, respectively. The dust layer of total column burden 100 mg m^{-2} has mass median diameter of 3.5 μm. The optical depth τ, asymmetry factor g, and single-scattering albedo ω are obtained by Mie calculations and then averaged over the solar wavelength region by

$$A = \frac{\int A(\lambda) W(\lambda) d\lambda}{\int W(\lambda) d\lambda} \quad (4)$$

where A represents τ, g, or ω, and $W(\lambda)$ is TOA incident solar flux. The values of $W(\lambda)$ are given by *Fröhlich and London* [1986]. The upscatter fraction β is calculated using an approximate relation, $\beta = \frac{1}{2}\left(1 - \frac{7g}{8}\right)$ [*Wiscombe and Grams*, 1976], which is the global mean value. For the dust aerosol parameters assumed, we obtain $\tau = 0.056$, $\beta = 0.18$, and $\omega = 0.89$.

In Figure 8, three cases are considered: (1) all aerosol above cloud ($\tau_3 = 0$), (2) all aerosol below cloud ($\tau_1 = 0$), and (3) aerosol located both above and below cloud, with $\tau_1 = \tau_3$. The critical value of ω is sensitive to the location of the aerosol layers for either type of cloud. For a surface albedo of 0.15, ω_{crit} is largest (about 0.98) when all aerosol lies above the cloud layer, as in this case even a small amount of aerosol absorption leads to heating; ω_{crit} is smallest when all aerosols are located below cloud (about 0.68 at $r_S = 0.15$), because only a fraction of incoming radiation reaches the aerosol layer. Consequently, the absorbing component of the particles must be quite substantial to lead to heating. When surface albedo exceeds about 0.5, the aerosol always leads to a heating effect regardless of the value of ω, the reason for which is absorption by surface and cloud. When an aerosol layer is present and surface albedo is high, the surface absorbs more radiation [*Haywood and Shine*, 1997]. According to our definition of TOA aerosol forcing, even though particles are nonabsorbing ($\omega = 1$), $-(F^d_{\mathrm{TOA}} \uparrow - F^0_{\mathrm{TOA}} \uparrow)$ is positive. Similarly, absorption by cloud also leads to positive aerosol forcing.

Since the parameters of the dust aerosol used for Figure 8 are the same as those in Figure 2, one can explain the TOA cooling and heating effects shown in Figure 2 by comparing ω and ω_{crit}. The spectrally averaged single-scattering albedo of the dust aerosol is $\omega = 0.89$. It can be seen that ω is always smaller than ω_{crit} for the case with all aerosol above cloud, which explains heating by a dust layer at 3-6 km in Figure 2. When all aerosol is below cloud, the curve for ω_{crit} crosses over $\omega = 0.89$ at a surface albedo of about 0.25, which is in approximate in agreement with the result shown in Figure 2; TOA forcing of the dust layer at 0-1 km changes from cooling to heating at a surface albedo of 0.22. We do not compare the case with aerosol both above and below the cloud layer in Figure 8 with that in Figure 2 because dust is assumed to exist within the cloud layer in the calculations of Figure 2, whereas no aerosol is assumed inside the

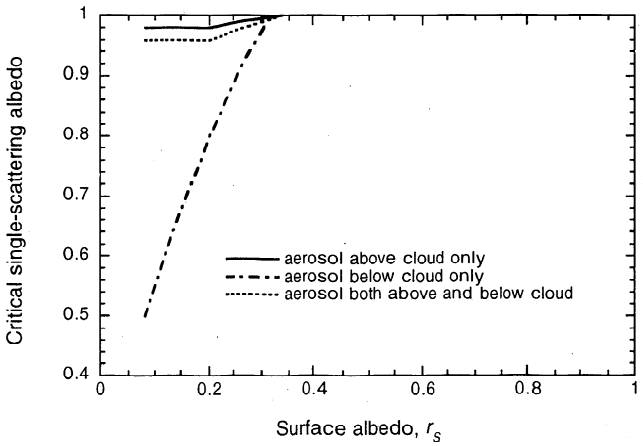

Figure 8. Critical single-scattering albedo ω_{crit} as a function of surface albedo and location of the dust layer. The 500 m thick cloud layer has liquid water content of 0.2 g m^{-3} and effective droplet radius 10 μm. $r_2 = 0.61$ and $t_2 = 0.32$. Total column burden of the dust layer is 100 mg m^{-2} and mass median diameter is 3.5 μm (the same as in Figure 2).

cloud layer in deriving ω_{crit}, although the difference is expected to be small.

It should be mentioned that in the above analysis, water vapor and Rayleigh scattering have been neglected for simplicity. This treatment should not lead to significant error since TOA forcing depends on the difference in planetary albedo instead of on the absolute value of planetary albedo.

7. Conclusion

The present work studies the sensitivity of diurnal average mineral dust forcing (TOA and surface) to the imaginary part of dust refractive index, dust particle size, dust altitude, dust optical depth, surface albedo, and the presence or absence of clouds. The sign of net dust forcing (shortwave plus longwave) at TOA depends on surface albedo, particle size, k (imaginary part of refractive index), and the presence or absence of clouds. Results show that low surface albedo and small particle size can produce negative forcing (cooling) under clear sky conditions, which is consistent with the results obtained by *Tegen and Lacis* [1996] and *Tegen et al.*, [1996]. At the surface, shortwave forcing always leads to cooling, and longwave forcing always leads to heating.

The presence of a low-level stratus cloud greatly alters both shortwave and longwave forcing by mineral dust from the values under clear-sky condition. Though longwave forcing is important under clear-sky condition [*Sokolik et al.*, 1998], it becomes practically negligible when clouds are present. Surface forcing in the presence of a cloud always leads to cooling and is greatly reduced in magnitude compared with clear-sky shortwave forcing. The sign of cloudy sky TOA forcing by dust is determined by the critical single-scattering albedo derived in this study.

Sensitivity studies show the following results:

1. Net TOA forcing is more sensitive to k, the imaginary part of the dust refractive index, than net surface forcing, no matter whether a cloud layer is present or not.
2. Clear-sky shortwave forcing (TOA and surface) is not sensitive to the altitude of the dust layer, but clear-sky longwave forcing (TOA and surface) and cloudy sky TOA shortwave forcing are quite sensitive to it.
3. Shortwave forcing (TOA and surface) under clear-sky conditions is more sensitive to dust mass median diameter than that under cloudy sky conditions. Longwave forcing is not sensitive to particle size.
4. All forcings are sensitive to dust optical depth except cloudy-sky longwave forcing.

Appendix: Derivation of Critical Single-Scattering Albedo for Cloud and Aerosol Layers

Consider the aerosol and cloud layers shown in Figure 7. For optically thin aerosol layers the reflectance and transmittance are given by [*Coakley and Chylek*, 1975; *King and Harshvardhan*, 1986]

$$r_1 = \frac{\tau_1 \omega_1 \beta_1(\mu_0)}{\mu_0} \tag{A1}$$

$$t_1 = 1 - \frac{\tau_1}{\mu_0}\left[1 - \omega_1 + \omega_1 \beta_1(\mu_0)\right] \tag{A2}$$

$$r_3 = \frac{\tau_3 \omega_3 \beta_3(\mu_0)}{\mu_0} \tag{A3}$$

$$t_3 = 1 - \frac{\tau_3}{\mu_0}\left[1 - \omega_3 + \omega_3 \beta_3(\mu_0)\right] \tag{A4}$$

where μ_0 is the cosine of solar zenith angle. The spherical reflectances and transmissions are obtained by integration of equations (A1)-(A4) over all angles of incoming radiation [*Chylek and Wong*, 1995]. We obtain

$$r_1 = 2\tau_1 \omega_1 \beta_1 \tag{A5}$$

$$t_1 = 1 - 2\tau_1 + 2\omega_1(1 - \beta_1)\tau_1 \tag{A6}$$

$$r_3 = 2\tau_3 \omega_3 \beta_3 \tag{A7}$$

$$t_3 = 1 - 2\tau_3 + 2\omega_3(1 - \beta_3)\tau_3 \tag{A8}$$

where

$$\beta_i = \int_0^1 \beta_i(\mu_0) d\mu_0 \qquad i = 1,3$$

By using the adding method [*Liou*, 1980], the combined reflectance and transmittance for layers 1 and 2 are

$$r_{12} = r_1 + \frac{r_2 t_1^2}{1 - r_1 r_2} \tag{A9}$$

$$t_{12} = \frac{t_1 t_2}{1 - r_1 r_2} \tag{A10}$$

Then regarding layers 1 and 2 as a single layer, we get the combined reflectance and transmittance of layers 1, 2, 3 as

$$r_{123} = r_{12} + \frac{r_3 t_{12}^2}{1 - r_{12} r_3} \tag{A11}$$

$$t_{123} = \frac{t_{12} t_3}{1 - r_{12} r_3} \tag{A12}$$

Similarly, the combined reflectance of layers 1, 2, 3 and the surface is

$$r_{123S} = r_{123} + \frac{r_S t_{123}^2}{1 - r_{123} r_S} \tag{A13}$$

Using equations (A5)-(A8) in (A9)-(A13) and neglecting terms involving τ_1^2 and $\tau_1 \tau_2$, one obtains

$$r_{12} \cong 2\tau_1 \omega_1 \beta_1 + r_2\left[1 - 4\tau_1 + 4\omega_1(1 - \beta_1)\tau_1 + 2\tau_1 \omega_1 \beta_1 r_2\right] \tag{A14}$$

$$t_{12} \cong \left[1 - 2\tau_1 + 2\omega_1(1 - \beta_1)\tau_1 + 2\tau_1 \omega_1 \beta_1 r_2\right] t_2 \tag{A15}$$

$$r_{123} \cong r_{12} + 2\tau_3 \omega_3 \beta_3 t_2^2 \tag{A16}$$

$$t_{123} \cong t_2\left[1 - 2\tau_1 + 2\omega_1(1 - \beta_1)\tau_1 + 2\tau_1 \omega_1 \beta_1 r_2 - 2\tau_3 + 2\omega_3(1 - \beta_3)\tau_3 + 2\tau_3 \omega_3 \beta_3 r_2\right] \tag{A17}$$

$$r_{123S} = r_{123}(1 + r_S^2 t_2^2) - r_S^2 r_2 t_2^2 + r_S t_2^2 (1 + r_S r_2)[1 - 4\tau_1 + 4\omega_1(1 - \beta_1)\tau_1 + 4\tau_1\omega_1\beta_1 r_2 - 4\tau_3 + 4\omega_3(1 - \beta_3)\tau_3 + 4\tau_3\omega_3\beta_3 r_2] \quad \text{(A18)}$$

If we let $\tau_1 + \tau_3 = \tau$, the total optical depth of the aerosol layer, $\beta_1 = \beta_3 = \beta$, and $\omega_1 = \omega_3 = \omega$, then

$$r_{123S} = (1 + r_S^2 t_2^2)\{2\tau_1\omega\beta + r_2[1 - 4\tau_1 + 4\omega(1 - \beta)\tau_1 + 2\tau_1\omega\beta r_2] + 2\tau_3\omega\beta t_2^2\} - r_S^2 r_2 t_2^2 + r_S t_2^2 (1 + r_S r_2)[1 - 4\tau + 4\omega(1 - \beta)\tau + 4\tau\omega\beta r_2] \quad \text{(A19)}$$

In the absence of aerosols the reflectance of the cloud-surface system is

$$r_{cs} = r_2 + \frac{r_S t_2^2}{1 - r_2 r_S} \quad \text{(A20)}$$

The change in reflectance as a result of the presence of the aerosol layers is $\Delta r_p = r_{123S} - r_{cs}$. Setting $\Delta r_p = 0$ leads to the desired expression for the critical single-scattering albedo of the aerosol, i.e., the value of ω at which Δr_p changes sign,

$$\omega_{crit} = \frac{\left(r_2 + \frac{r_S t_2^2}{1 - r_2 r_S}\right) + r_S^2 r_2 t_2^2 - r_2(1 + r_S^2 t_2^2)(1 - 4\tau_1) - r_S t_2^2 (1 + r_S r_2)(1 - 4\tau)}{2(1 + r_S^2 t_2^2)[\tau_1\beta + 2r_2(1 - \beta)\tau_1 + r_2^2\tau_1\beta + \tau_3\beta t_2^2] + r_S t_2^2 (1 + r_S r_2)[4(1 - \beta)\tau + 4\beta\tau_2]} \quad \text{(A21)}$$

Acknowledgment. This work was supported by National Science Foundation grant ATM-9614105.

References

Carlson, T. N., and S. Benjamin, Radiative heating rates for Sahara dust, *J. Atmos. Sci., 37,* 193-213, 1980.

Cess, R. D., Nuclear war: Illustrative effects of atmospheric smoke and dust upon solar radiation, *Clim. Change, 7,* 237-251, 1985.

Chylek, P., and J. T. Kiehl, Sensitivities of radiative-convective climate models, *J. Atmos. Sci., 38,* 1105-1110, 1981.

Chylek, P., and J. Wong, Effect of absorbing aerosols on global radiation budget, *Geophys. Res. Lett., 22,* 929-931, 1995.

Chylek, P., and J. A. Coakley, Aerosols and climate, *Science, 183,* 75-77, 1974.

Coakley, J., and P. Chylek, The two-stream approximation in radiative transfer: Including the angle of incident radiation, *J. Atmos. Sci., 32,* 409-418, 1975.

Crisp, D., Absorption of sunlight by water vapor in cloudy conditions: A partial explanation for the cloud absorption anomaly, *Geophys. Res. Lett., 24,* 571-574, 1997.

Dentener, F. J., G. R. Carmichael, Y. Zhang, J. Lelieveld, and P.J. Crutzen, Role of mineral aerosol as a reactive surface in the global troposphere, *J. Geophys. Res., 101,* 22, 869-22, 889, 1996.

Fröhlich, C., and J. London, Revised instruction manual on radiation instruments and measurements, World Clim. Res. Program (WCRP), *Pub. Ser. 7,* WMO *TD 149,* World Meteorol. Organ., Geneva, 1986.

Fu, Q., and K. N. Liou, Parameterization of the radiative properties of cirrus clouds, *J. Atmos. Sci., 50,* 2008-2025, 1993.

Hansen, J., M. Sato, and R. Ruedy, Radiative forcing and climate response, *J. Geophys. Res., 102,* 6831-6864, 1997.

Haywood, J. M., and K. P. Shine, Multi-spectral calculations of the direct radiative forcing of tropospheric sulfate and soot aerosols using a column model, *Q. J. R. Meteorol. Soc., 123,* 1907-1930, 1997.

King, M. D., and Harshvardhan, Comparative accuracy of selected multiple scattering approximations, *J. Atmos. Sci., 43,* 784-801, 1986.

Lacis, A.A., and M.I. Mishchenko, Climate forcing, climate sensitivity, and climate response: A radiative modeling perspective on atmospheric aerosols, in *Aerosol Forcing of Climate,* edited by R. Charlson and J. Heintzenberg, pp. 11-42, John Wiley, New York, 1995.

Liou, K. N., *An Introduction to Atmospheric Radiation,* Academic, San Diego, Calif., 1980.

Mishchenko, M.I., Light scattering by size-shape distributions of randomly oriented axially symmetric particles of a size comparable to a wavelength, *Appl. Opt., 32,* 4652-4666, 1993.

Mishchenko, M.I., and L.D. Travis, Light scattering by polydispersions of randomly oriented spheroids with sizes comparable to wavelengths of observation, *Appl. Opt., 33,* 7206-7225, 1994.

Patterson, E.M., D.A. Gillette, and B.H. Stockton, Complex index of refraction between 300 and 700 nm for Saharan aerosols, *J. Geophys. Res. 82,* 3151-3160, 1977.

Ramanathan, V., Interactions between ice-albedo, lapse-rate and cloud-top feedbacks: An analysis of the nonlinear response of a GCM climate model, *J. Atmos. Sci., 34,* 1885-1897, 1977.

Ramaswamy, V., and J.T. Kiehl, Sensitivities of the radiative forcing due to large loading of smoke and dust aerosols, *J. Geophys. Res., 90,* 5597-5613, 1985.

Seinfeld, J. H., and S. N. Pandis, *Atmospheric Chemistry and Physics.* Wiley, New York, 1997.

Sokolik, I. N., and G. S. Golitsyn, Investigation of optical and radiative properties of atmospheric dust aerosols, *Atmos. Environ., 27A,* 2509-2517, 1993.

Sokolik, I. N., and O. B. Toon, Direct radiative forcing by anthropogenic mineral aerosols, *Nature, 381,* 681-683, 1996.

Sokolik, I. N., A. V. Andronova, and T. C. Johnson, Complex refractive index of atmospheric dust aerosols, *Atmos. Environ., 27A,* 2495-2502, 1993.

Sokolik, I.N., O.B. Toon, and R.W. Bergstrom, Modeling the radiative characteristics of airborne mineral aerosols at infrared wavelengths, *J. Geophys. Res. 103,* 8813-8826, 1998.

Tegen, I., and I. Fung, Modeling of mineral dust in the atmosphere: Sources, transport, and optical thickness, *J. Geophys. Res., 99,* 22,897-22,914, 1994.

Tegen, I., and A. A. Lacis, Modeling of particle size distribution and its influence on the radiative properties of mineral dust aerosol, *J. Geophys. Res., 101,* 19,237-19,244, 1996.

Tegen, I., A. A. Lacis, and I. Fung, The influence on climate forcing of mineral aerosols from disturbed soils, *Nature, 380,* 419-422, 1996.

Wiscombe, W. J., and G. W. Grams, The backscattered fraction in two-stream approximations, *J. Atmos. Sci., 33,* 2440-2451, 1976.

H. Liao, Department of Environmental Engineering Science, California Institute of Technology, Pasadena, CA 91125. (email: hong@cco.caltech.edu)

J.H. Seinfeld, Division of Engineering and Applied Science, California Institute of Technology, Pasadena, CA 91125. (email: seinfeld@cco.caltech.edu)

(Received January 26, 1998; revised September 9, 1998; accepted September 23, 1998)